OXFORD

Human Molecular Genetics, 2016, 1–15

doi: 10.1093/hmg/ddv514
Advance Access Publication Date: 18 December 2015
Original Article

ORIGINAL ARTICLE

The apical ectodermal ridge of the mouse model of ectrodactyly *Dlx5;Dlx6*$^{-/-}$ shows altered stratification and cell polarity, which are restored by exogenous Wnt5a ligand

Daniele Conte[1], Giulia Garaffo[1], Nadia Lo Iacono[2], Stefano Mantero[2], Stefano Piccolo[3], Michelangelo Cordenonsi[3], David Perez-Morga[4], Valeria Orecchia[1], Valeria Poli[1] and Giorgio R. Merlo[1,*]

[1]Department of Molecular Biotechnology and Health Sciences, University of Torino, Torino, Italy, [2]Human Genome Department, Istituto Tecnologie Biomediche, CNR Milano, Italy, [3]Department of Molecular Medicine, University of Padova, Padova, Italy and [4]Laboratoire de Parasitologie Moléculaire, IBMM-DBM, Université Libre de Bruxelles, B-6041 Gosselies, Belgium

*To whom correspondence should be addressed at: Department of Molecular Biotechnology and Health Sciences, Via Nizza 52, 10126 Torino, Italy. Tel: +39 0116706449; Fax: +39 0116706432; Email: giorgioroberto.merlo@unito.it

Abstract

The congenital malformation split hand/foot (SHFM) is characterized by missing central fingers and dysmorphology or fusion of the remaining ones. Type-1 SHFM is linked to deletions/rearrangements of the *DLX5–DLX6* locus and point mutations in the *DLX5* gene. The ectrodactyly phenotype is reproduced in mice by the double knockout (DKO) of *Dlx5* and *Dlx6*. During limb development, the apical ectodermal ridge (AER) is a key-signaling center responsible for early proximal–distal growth and patterning. In *Dlx5;6* DKO hindlimbs, the central wedge of the AER loses multilayered organization and shows down-regulation of FGF8 and Dlx2. In search for the mechanism, we examined the non-canonical Wnt signaling, considering that *Dwnt-5* is a target of *distalless* in Drosophila and the knockout of Wnt5, Ryk, Ror2 and Vangl2 in the mouse causes severe limb malformations. We found that in *Dlx5;6* DKO limbs, the AER expresses lower levels of *Wnt5a*, shows scattered β-catenin responsive cells and altered basolateral and planar cell polarity (PCP). The addition of Wnt5a to cultured embryonic limbs restored the expression of AER markers and its stratification. Conversely, the inhibition of the PCP molecule c-jun N-terminal kinase caused a loss of AER marker expression. *In vitro*, the addition of Wnt5a on mixed primary cultures of embryonic ectoderm and mesenchyme was able to confer re-polarization. We conclude that the *Dlx*-related ectrodactyly defect is associated with the loss of basoapical and PCP, due to reduced *Wnt5a* expression and that the restoration of the Wnt5a level is sufficient to partially reverts AER misorganization and dysmorphology.

Received: November 4, 2015. **Revised and Accepted:** December 10, 2015

Introduction

Ectrodactyly, or split-hand/foot malformation (SHFM, MIM 183600) consists in the absence of the distal portion of the central rays of upper and lower limbs, resulting in a deep medial cleft, missing or hypoplastic central fingers and fusion of the lateral ones (reviewed in 1,2). SHFM comprises both syndromic or isolated forms, linked to six loci (3–5). The most common non-syndromic form is SHFM type-1, associated to variable deletions on chromosome 7q21. The minimal commonly deleted region includes the homeogenes *DLX5* and *DLX6* (2). Recently a point mutation in the DNA-binding domain of *DLX5* (Q178P) has been reported in a SHFM-1 family with a recessive transmission, co-segregating with the limb malformations (6). SHFM type-4 (MIM 605289) is considered a variant of the ectodermal dysplasia-ectrodactyly cleft lip/palate (EEC) syndrome, in which only the limb phenotype is present. Indeed SHFM-4 and EEC are caused by mutations in the *p63* gene, and in 50 unrelated patients with isolated SHFM type-5 had mutations in *p63*, suggesting that these may account for ~10% of sporadic SHFM cases (7). Of note, SHFM type-6 (MIM 225300) has been linked to homozygous loss of the *WNT10B* gene (3,8–10).

In the mouse, the double knockout (DKO) of *Dlx5* and *Dlx6* leads to ectrodactyly of the hindlimbs (11,12), fully confirming the molecular and genetic basis of SHFM-1. The developmental defect originates from misfunction and misorganization of the cells of the apical ectodermal ridge (AER), a specialized region of the ectoderm at the Dorsal–Ventral (Do–Ve) margin of the developing limb (13). Evidence has been collected that, starting ~E10.5–E11 the expression of several AER markers is lost in the central wedge of the AER, and at about the same time the first signs of dysmorphology are visible. Such is the case of signaling molecules and transcription factors, known to be critically involved in the AER function to maintain proliferation of the progress zone. Considering that Dlx5 and Dlx6 code for transcription factors, and that their expression is largely restricted to the AER, the *Dlx5;6* DKO defect can be summarized as a cell-autonomous failure of the central AER to maintain and express morphogenetic signals and to finely regulate p63 (14,15).

Dlx genes code for homeodomain-containing transcription factors that are the vertebrate homologs of Drosophila *distalless* (*dll*), a gene required for the specification of leg (and other appendages) distal elements. In *dll* hypomorphic mutant flies, a variable set of phenotypes is observed depending on the mutation, ranging from fusion of the distal segments (mild mutants) to complete loss of distal and medial leg segments (severe mutants) (16,17). In search for Dlx transcriptional targets that might clarify the molecular and cellular basis of ectrodactyly, we speculated that targets of *dll* in the Drosophila embryo could also be targets of *Dlx* genes in the mammalian embryo. Among them, *Dwnt-5* and its closest mammalian homolog *Wnt5a* (18) caught our attention for several reasons: (1) *Wnt5a* is expressed in the limb bud AER and mesenchyme in a distal-high to proximal-low gradient, at the same time as *Dlx5*, *Dlx6* and *p63*; (2) *Wnt5a*$^{-/-}$ mice display evident Proximal–Distal (Pr–Di) limb defects, consisting in short metacarpal elements, truncation of proximal elements and absence of phalanges (19,20) and (3) the loss of the non-canonical Wnt receptors Ryk and Ror2 causes limb developmental defects similar to those of *Wnt5a* mutants (21–23).

Wnt5a codes for a ligand of the Wnt family, which activates the β-catenin-independent planar cell polarity (PCP) pathway (18,24,25), recruiting Rho, cdc42, Vangl2 and the c-jun N-terminal kinase (JNK) (26–28). The loss of *Vangl2* as well as other components of PCP results in Pr–Di limb defects (26,29–31). At the cellular level the role of Wnt5a is not fully understood; recent findings indicate that it takes part in developmental processes such as oriented cell migration and division (32), establishment of PCP and convergent extension (CE). Since the AER forms via CE (33–35), we raised the hypothesis that a Wnt5a-activated PCP pathway is downstream of *Dlx5* and *Dlx6* and its perturbation causes altered AER organization and function, resulting in ectrodactyly. Notably, Wnt5a has been shown to be a transcriptional target of Dlx5 in the brain (36).

In this work, we sought to identify novel targets of Dlx5, examine the function of Wnt5a and clarify the cellular pathogenesis of the AER misfunction in the *Dlx5;6* DKO model of ectrodactyly. The results show that the *Dlx*-caused ectrodactyly is associated with the loss of *Wnt5a* expression in the central AER of limb buds, which results in altered basoapical and PCP. Exposure of *Dlx5;6* DKO mutant limbs to exogenous Wnt5a rescues AER stratification and expression of specific markers.

Results

Histology of the AER in *Dlx5;6* DKO limbs

The central sector of the AER of *Dlx5;6* DKO limbs, at early embryonic ages (E10.5–E11.5) has been previously shown to be defective in the expression of molecules such as *Fgf8*,*Msx2* and *Bmp4* (11,12,37). In addition, whole-mount *in situ* hybridization with a probe detecting the *Dlx2* mRNA showed the same altered expression pattern (Fig. 1A). At slightly later ages (E12.5) a dysmorphology affecting the central sector of the *Dlx5;6* DKO hindlimbs is clearly visible (Fig. 1B).

Defective AER often shows altered stratification. Indeed we have previously reported a reduced stratification of the central wedge of the AER cells in *Dlx5;6* DKO limbs (14). We also showed that p63, a marker of ectodermal stem/progenitor cells required for skin stratification (38), is still expressed in AER and ectoderm cells of *Dlx5;6* mutant limbs, although at reduced level. Thus, we decided to further examine histological parameters of organization and integrity of the AER cells in the developing limbs. We focused on the embryonic ages E10.5–E11.5, e.g. prior to the onset of ectrodactyly and prior to overt changes in the expression of AER markers. We also examined the limbs at the age E12.5, when morphological and molecular defects first appear. Limbs were sectioned parallel to the Do–Ve plane (scheme in Fig. 1D). We initially immunostained for E-cadherin and ZO-1 to examine basoapical polarity. E-cadherin is a general epithelial marker present mostly at the basolateral membrane of epithelial cells, while ZO-1 stains the mostly apical lateral membrane. The AER of the *Dlx5;6* DKO hindlimbs appeared normal in lateral sectors; however, in the central sector the AER appeared composed of a less stratified epithelium. E-cadherin staining showed a normal expression on the lateral cell borders, a reduction of the basal expression and the appearance of apical expression (Fig. 1C). ZO-1 staining revealed the converse alteration: its expression was reduced in the apical position and appeared in the basal layer, absent in the normal limb control (Fig. 1C). We confirmed the altered basoapical polarity defect by staining for GM130, which recognizes the Golgi organelle. This is generally located in a supra-nuclear position in epithelial cells. Combining immunostaining for GM130 and DAPI staining (for nuclei), we determined the overall orientation of AER cells relative to the Do–Ve and Pr–Di directions. In normal limbs we observed that nearly all the AER cells showed a basoapical orientation parallel to the Pr–Di orientation and parallel to the Do–Ve plane, with the GM130 fluorescent staining always apical with respect to the nuclei. In

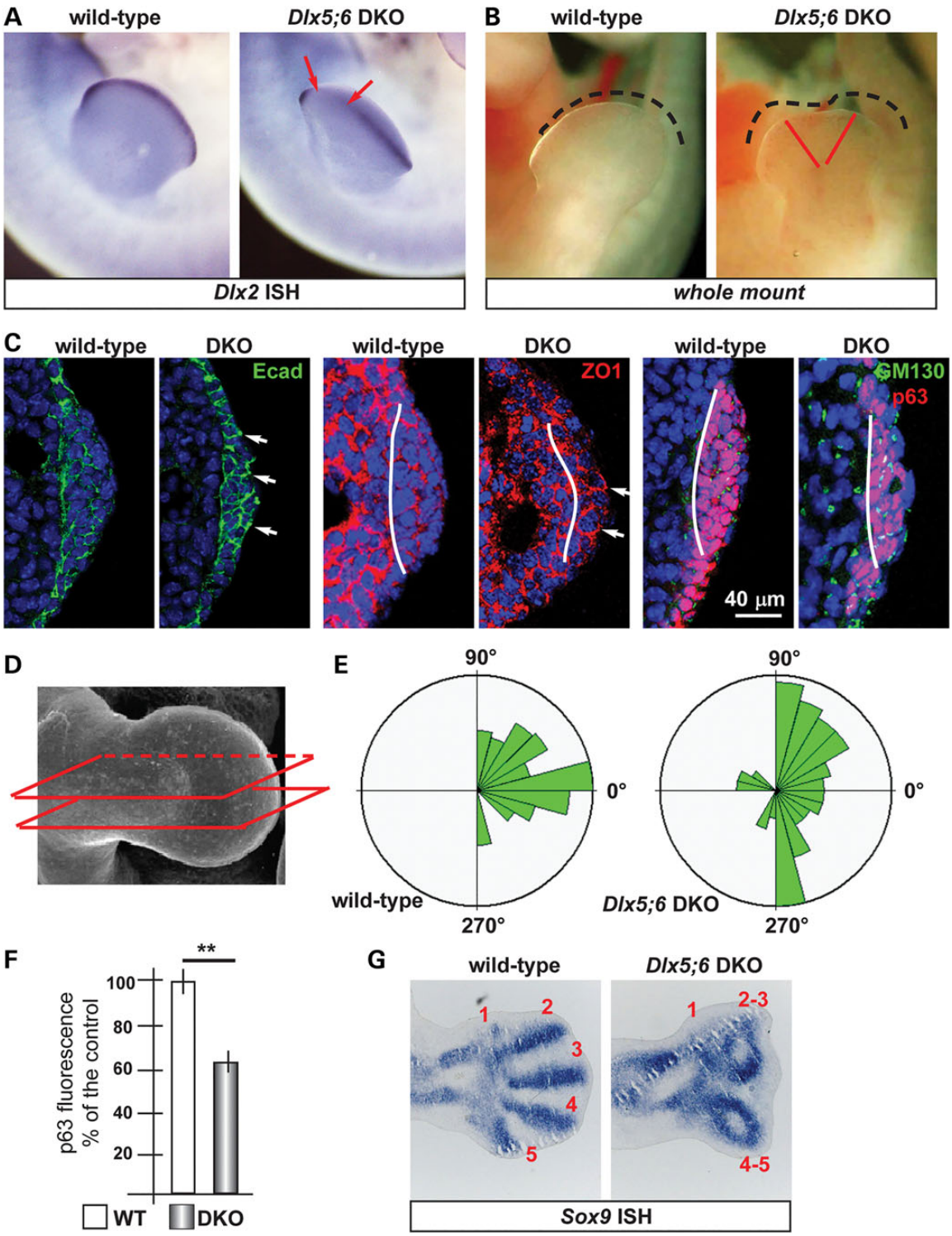

Figure 1. Histology of the AER of limbs of *Dlx5;6* DKO mouse embryos. (**A**) Whole-mount *in situ* hybridization on WT (left) and *Dlx5;6* DKO (right) hindlimbs at age E 11.5, to detect *Dlx2* mRNA. Red arrows indicate the beginning and the end of a 'reduced expression' region. (**B**) General appearance of WT (left) and *Dlx5;6* DKO (right) hindlimbs, at the age E11.5, in whole-mount bright field examination. Red-dotted lines show the contour of the AER. (**C**) Immunostaining on sections of WT or *Dlx5;6* DKO hindlimbs (respectively on the left and on the right of each pair) to detect E-cadherin (left), ZO-1 (middle), GM130 and p63 (right). While lines indicate the contour of the AER. Arrows indicate cells with clearly expression pattern defect. Scale bars are inserted. (**D**) Scheme of the section plane. (**E**) Rosette diagram of the orientation of the Golgi with respect to the surface in WT and *Dlx5;6* DKO limbs. (**F**) Quantification of p63 expression levels in WT and *Dlx* mutant limbs, expressed in percentage of the WT (=100%). Asterisk indicates statistical significance. (**G**) *In situ* hybridization on sections of WT (left) and *Dlx5;6* DKO (right) hindlimbs, to detect the *Sox9* mRNA. Red numbers indicate the digits, 1 is the thumb.

contrast, the AER cells of *Dlx5;6* DKO limbs were highly disoriented, with a large fraction of them showing the Nucleus-Golgi basoapical direction not parallel to the Pr–Di direction (Fig. 1D and E).

Chondrogenesis is defective in the central wedge of *Dlx5;6* DKO limbs

We then decided to examine the pattern of mesenchymal condensation in the developing limb buds, as an estimate of overall limb dysmorphogenesis. For this, we carried out whole-mount and section *in situ* hybridization to visualize *Sox9* expression. Indeed, *Sox9* is one of the earliest genes expressed in chondrogenic condensations and can be used as a marker to visualize skeletal patterning at early stages of development (39). Wild-type (WT) and *Dlx5;6* DKO limbs, at the age E11.5, were sectioned in a direction parallel to the Do–Ve symmetry plane. *Sox9* hybridization on normal E12.5 hindlimbs yielded signal corresponding to all five elements of the zeugopod (fingers), two elements of the autopod and a number of smaller *Sox9* expression domain corresponding to the carpal-metacarpal skeletal elements (Fig. 1F). In the *Dlx5;6* DKO hindlimbs, the same pattern of *Sox9* gene expression was observed corresponding to the autopod and the carpal-metacarpal elements. However, the zeugopod elements appeared disoriented, particularly in their most distal domain. The expression territory corresponding to Fingers 3 and 4 were bent, respectively, anteriorly and posteriorly, and apparently fused in their most distal position with Fingers 2 and 5 (Fig. 1F). Thus, as early as E12.5 and much prior to the appearance of mineralized skeletal elements, an ectrodactyly condition identical to the phenotype observed at E14.5 and later stages is already evident (12).

We (12–14) and others (11) have previously shown that in the central sector of the *Dlx5;6* DKO limbs expression of *Fgf8*, *Dlx2*, *Bmp4* and (in this study) *Wnt5a* mRNAs is reduced. Since FGF8 is considered the key mitogen for distal mesenchymal cells (40–43), we used BrdU incorporation to determine the number of proliferating cells in the AER and distal mesenchyme of WT and *Dlx5;6* DKO limbs. At the age E12.5, e.g. when the ectrodactyly is morphologically evident, the central AER and distal mesenchyme showed a significantly reduced number of BrdU+ nuclei (mutant AER versus WT –50%, mutant mesenchyme versus WT –60%), while the lateral AER and distal mesenchyme appeared normal (Supplementary Material, Fig. S1). Likewise, at the age E11.5, e.g. prior to limb dysmorphology, we observed a reduced number of BrdU+ cells in the central AER and distal mesenchyme (mutant AER versus WT –38%, mutant mesenchyme versus WT –31%) while in lateral sectors we observed no significant changes (Supplementary Material, Fig. S1). This result is in partial agreement with a previous report (11) in which, however, no changes were reported in the distal mesenchyme. We also determined the number of apoptotic cells in E11.5 WT with *Dlx5;6* DKO limb buds, by immunostaining for anti-activated Caspase3. Positive cells were seen in the AER and in the mesenchyme, as well as clustered in the posterior necrotic zone (44). The number Casp3+ cells in the AER, mesenchyme and necrotic zones did not significantly change in WT versus *Dlx5;6* DKO limbs (data not shown), as previously reported (11).

Expression of candidate Dlx5;Dlx6 targets

In search for targets of *Dlx* genes relevant for limb development, we first compared the mRNA abundance of genes known to cause ectrodactyly, or putatively linked to the malformation, in mice and human (4,5). We carried out real-time quantitative polymerase chain reaction (qPCR) on total RNA extracted from the central wedge of hindlimbs of WT or *Dlx5;6* DKO embryos, at the age E11.5. The mRNAs included *Wnt10b*, *Dactylyn*, *Np63* and *p63*. No significant change in the mRNA levels of these genes was detected (Fig. 2A and B). These genes were not further considered.

Secondly, we considered a set of mammalian homologs of genes known to be downstream target of Drosophila *dll*. The latest included *aristaless*, *barH1/barH2*, *bric-a-brac*, *dachshund*, *disconnected*, *Dwnt5*, *serrate*, *spalt* and *spineless* (16,17) (Supplementary Material, Table SII). The expression of these Drosophila genes is lost or reduced in *dll* mutant fly, either in the legs or in other appendages, with the exception of *Serrate* (*Jagged2* in vertebrates) which is instead up-regulated. Hoping to get clues on the possibility that their mammalian homologs may represent novel targets of Dlx5;Dlx6 potentially implicated in ectrodactyly, we examined the expression of the following: *Sall1*, *dachshund*, *Jagged2*, *Prx1*, *Prx2* and *Alx3* (Supplementary Material, Table SII). Two of these mRNAs, *Sall1* and *Prx1*, were found to be up-regulated in mutant limbs, while *Wnt5a* (the mammalian homolog of *D-wnt5*, a target of drosophila *dll*) was down-regulated (–45%) while all the other mRNAs were unchanged in the mutant limbs (Fig. 2A). Given the importance of Wnt5a for limbs development, we focused on this. *Sall1* and *Prx1* were expected to be down-regulated (45,46), and the loci are not associated with predicted DLX5-binding sites; for these reasons they were not further considered.

Thirdly, we considered the mRNAs coding for Wnt ligands. Several *Wnt* genes are expressed in the vertebrate embryonic limb buds, among these *Wnt3*, expressed in the AER and the entire limb ectoderm, *Wnt5a* and *Wnt5b*, expressed in both the AER and limb mesoderm in a high-distal to low-proximal gradient, Wnt7a, expressed in the dorsal ectoderm, and *Wnt11*. First, we analyzed abundance of the *Wnt3*, *Wnt5b* and *Wnt11* mRNAs by real-time qPCR on total RNA of embryonic hindlimbs at the age E11.5. The results indicate a decrease (–20%) of *Wnt3* expression and an increase (+20) of *Wnt11* expression in the central section of the AER in the *Dlx5;6* DKO limbs, compared with normal ones (Fig. 2B). We then examined the expression of the Wnt5a receptors *Ryk* and *Ror2* mRNAs, coding for Wnt5a receptors, and did not observe significant differences. Finally, we examined the expression of *RhoU* mRNA, coding for an atypical small-GTPase implicated in the Wnt signaling pathway (47), and observed a 60% reduced expression in the mutant limbs (Fig. 2B). *Wnt7a* was not examined since this molecule is known to play a role in Do–Ve patterning of the limb, which is unaffected in the *Dlx5;6* DKO limbs. As control, the level of *Dlx5* mRNA was examined and found to be completely abolished.

We confirmed the qPCR finding about Wnt5a, by carrying out *in situ* hybridization on sections of WT and *Dlx5;6* DKO limbs, at the age E11.5, with an RNA probe specific for *Wnt5a*. We observed a decreased hybridization signal specifically on the AER of *Dlx5;6* DKO limb, while in control limbs expression in the AER is evident (Fig. 2C).

Ectopic *Wnt*-β-catenin responsive cells in *Dlx5;6 DKO* limbs

Although widely proposed to use a β-catenin-independent pathway (48), Wnt5a has also been shown to promote β-catenin degradation, as the disruption of *Wnt5a* in the mouse leads to stabilization of β-catenin and the appearance of ectopic Wnt-β-catenin responsive cells in the developing limbs (20). To further support our previous findings, we sought a functional evidence of diminished Wnt5a activity in *Dlx5;6* DKO mutant limbs. We opted to use an *in vivo* β-catenin-reporter genetic system to

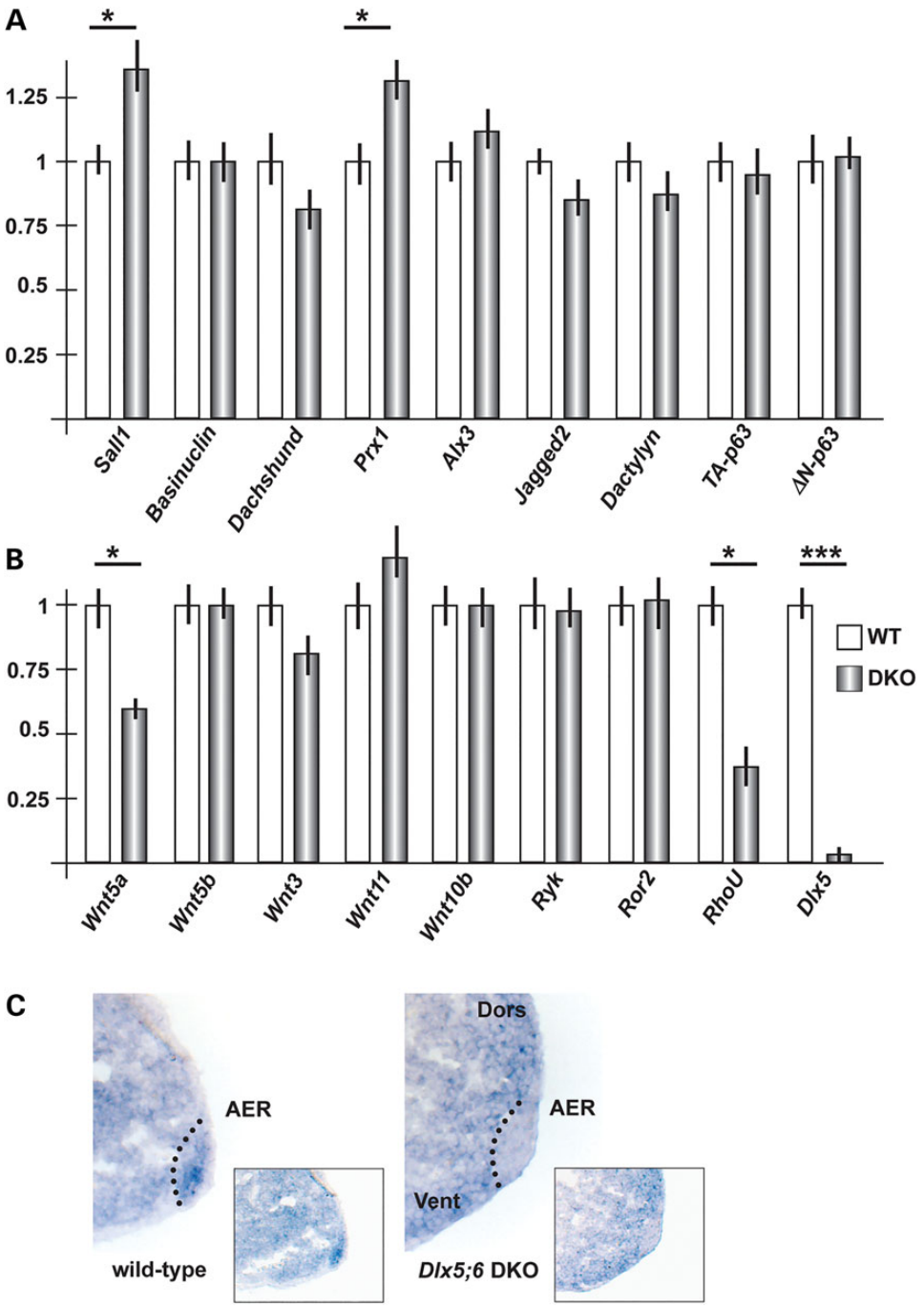

Figure 2. Expression of putative dll/Dlx targets in *Dlx5;6* DKO embryonic limbs. (**A**) Real-time qPCR to determine the relative abundance of putative Dlx targets, selected from the best homologs of dll targets in Drosophila. WT, open bars; Dlx mutant, patterned bars. The expression of the WT is normalized =1. Asterisks indicate statistical significance. (**B**) Real-time qPCR to detect the relative abundance of mRNAs coding for canonical and non-canonical Wnts, the *Ryk* and *Ror2* receptors and *RhoU*. (**C**) *In situ* hybridization on sections of WT and *Dlx5;6* DKO limbs, at the age E11.5. The AER is indicated with a dotted black line. Inserts show low-magnification images of the same.

visualize Wnt activity, namely the BAT-*LacZ* mouse (49). In this animal the *LacZ* reporter is expressed upon β-catenin activation, and a strong signal is detected in the AER. We cross-bred the *Dlx5;6* DKO animals with *BAT-LacZ* ones and proceeded to examine and quantify the β-gal+ cells in the limb buds of these embryos at the age E11.5. In WT or *Dlx5;6*$^{+/-}$ limbs, β-gal+ cells were seen along the length of the AER, with very few or none in non-AER positions, as expected (Fig. 3). No differences were observed when we compared WT and *Dlx5;6* DKO forelimbs (4 of 4), consistent the absence of malformations affecting them (11,12) (Fig. 3B). In contrast, the hindlimbs of *Dlx5;6* DKO embryos (4 of 5) showed numerous β-gal+ cells scattered dorsally and ventrally of the AER (Fig. 3A and E), while the total number of β-gal+ cells did not significantly change between the two genotypes (Fig. 3D). Thus, the loss of *Dlx5* and *Dlx6* leads to a scattering of the Wnt-β-catenin-responsive cells near the AER, an effect that is similar to that observed in the limbs of *Wnt5a*$^{-/-}$ mice (19,20).

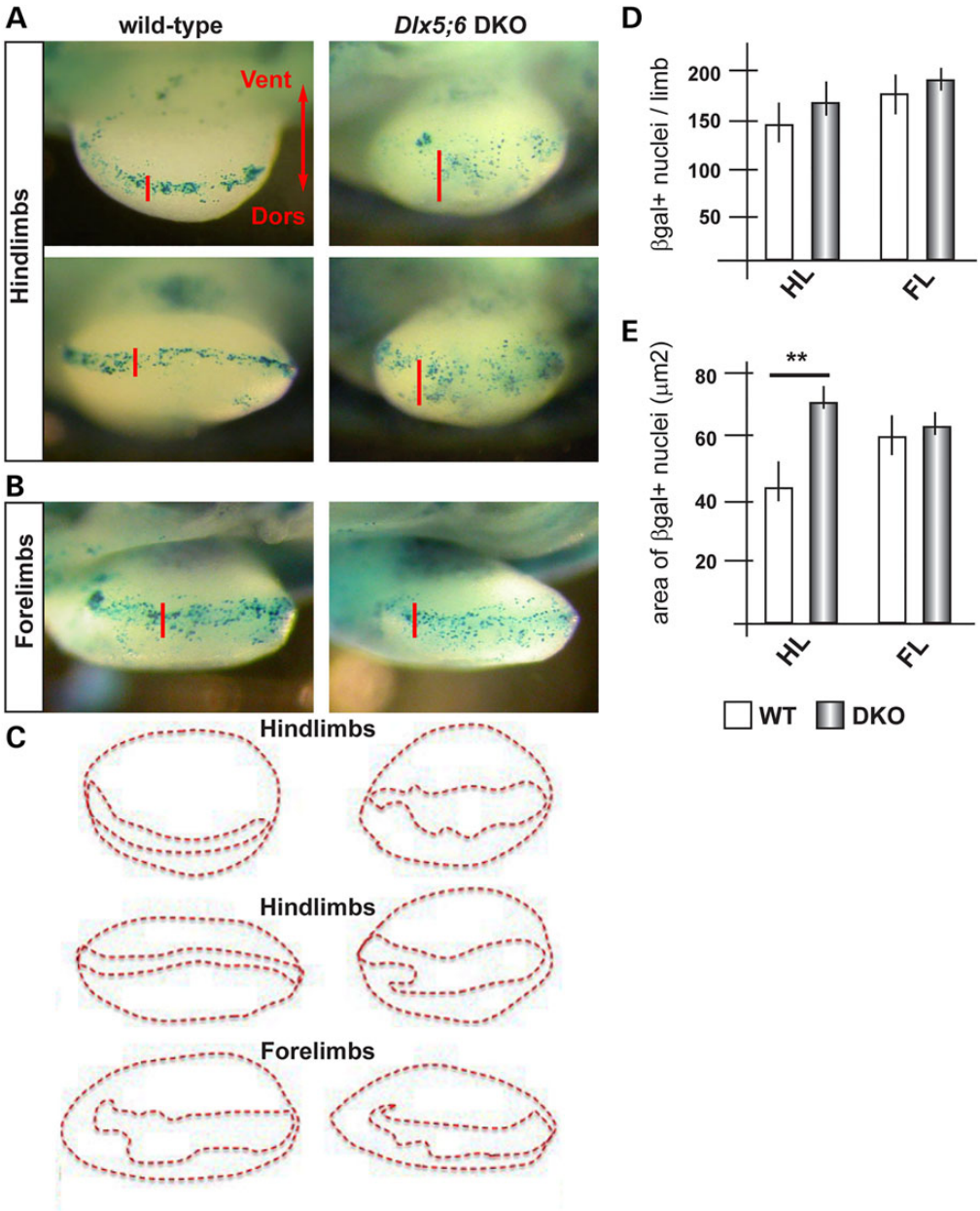

Figure 3. Wnt/βcatenin-responsive cells in normal and *Dlx5;6* DKO embryonic limbs. (**A**) Bright field images of X-gal-stained hindlimbs from WT (panels on the left) or *Dlx5;6* DKO (panels on the right) embryos, at the age E11.5. These embryos were also heterozygous for the transgene *BAT-lacZ*. Red bars indicate the Do–Ve distribution of the β-gal+ nuclei at or near the AER. (**B**) Same as in (A), but forelimbs are shown. (**C**) Contours of the areas occupied by β-gal+ nuclei (B), used for the analysis in (E). (**D** and **E**) Quantification of the number of β-gal+ nuclei per limb, in the two genotypes (D) and quantification of the Do–Ve distribution of the same (E) per area (C). WT, open bars; Dlx mutant, patterned bars. Asterisks indicate statistical significance.

Wnt5a activates a basolateral and a PCP on primary cultures of embryonic ectoderm cells

Wnt5a and PCP have been implicated in the oriented migration and cell division of the limb mesenchymal cells (32); however, little is known about the overlaying ectoderm cells. Due to their peculiar position at the Do–Ve margin, the AER cells are likely to show PCP, and the multilayered organization of the AER is attained by CE, a cellular process that uses the PCP pathway. Furthermore, the AER might be the prime (autocrine) target of Wnt5a, since *Wnt5a* expression is highest in this territory. Thus, we set forth to collect evidence that the altered expression of *Wnt5a* in the mutant *Dlx5;6* DKO limbs might be associated with changes in features linked to the establishment of basoapical or planar polarity of the AER cells.

We examined whether Wnt5a indeed exerts such function directly on embryonic ectoderm cells, derived from the limbs. We cultured primary limb ectoderm cells on laminin-coated dishes, in which an agarose drop containing *Wnt5a*-expressing cells was inserted. Non-expressing cells were used as negative control. After 48 h in culture, we assessed cell orientation by staining with anti-GP130 (for the Golgi) or anti γ-tubulin (for the centrosome/basal body) antibodies, and counterstaining with DAPI (for the nuclei). Within the mixed cultures the ectodermal cells are easily distinguished from the embryonic fibroblasts for

their morphology, their organization in clumps and their positivity for p63 and E-cadherin immunostaining. The orientation was reported as a distribution along the entire 360° range. In control samples, in which Wnt5a was not added, the AER cells tended to be randomly oriented (Fig. 4). In contrast, the addition of Wnt5a resulted in a large fraction of ectodermal cells to orient their Golgi toward the center of the cell clump, e.g. assuming a seeming correct basoapical polarity. This organization is likely due to tensile forces and is highly reminiscent of what other authors have documented when mixing-sorting primary embryonic cells *in vitro* (50). These data indicate that Wnt5a contributes to the establishment of basoapical and planar polarity in cultured ectodermal cells from WT limbs.

It has been proposed that cells in which PCP is impaired, tend to acquire abnormal cell shapes. Specifically, normal AER cells of limb buds ~E10.5–E11 appear polygonal in shape, with four– to five sides and sharp angles, and present numerous microvilli. The same cells in which the PCP is affected loose the polygonal shape, acquire instead a curvy shape with rounded angles, and lack microvilli (35). We, therefore, re-examined the morphology of AER cells of WT and *Dlx5;6* DKO embryos, at the age E11, obtained by SEM (14), and found that *Dlx5;6* DKO cells of the AER

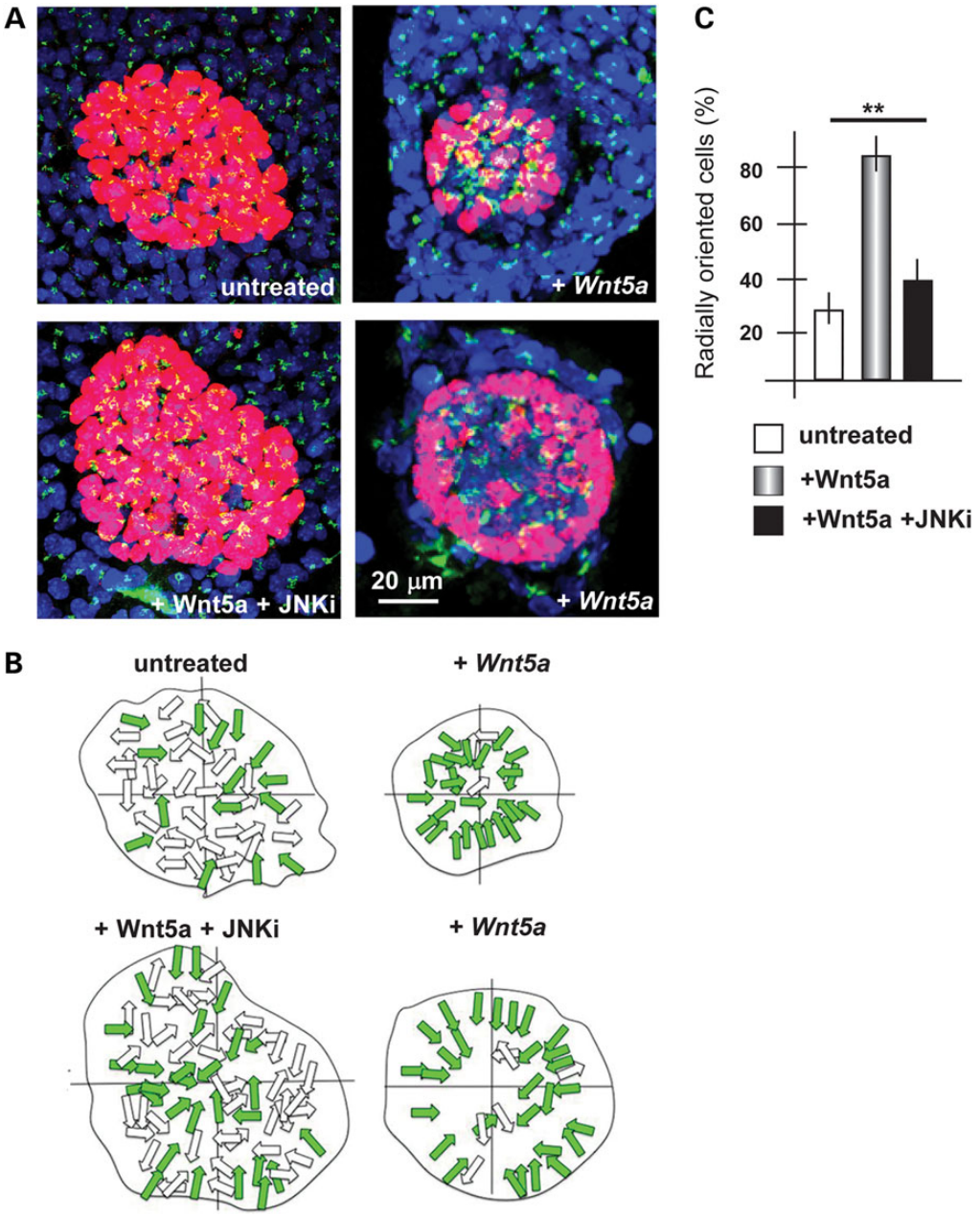

Figure 4. Orientation of cultured primary ectodermal cells in response to Wnt5a. (**A**) Fluorescent micrographs of clumps of ectodermal cells, immunostained for p63 (red) and GM130 (green). Treatments are indicated below each panel. Scale bar is reported. (**B**) The schematic diagram of radially oriented (colored arrows) and non-radially oriented (open arrows) cells in each condition. (**C**) Quantification of the number of p63+ cells with the orientation of the Golgi apparatus radially respect to the nucleo, with respect to the total p63+ cells. Untreated, open bars; treated with Wnt5a, patterned bars; treated with Wnt5 + JNKi, solid black bars. Asterisks indicate the statistical significance.

are often larger, lack sharp angles and present fewer microvilli, while the corresponding WT AER cells display all the expected morphological features (Supplementary Material, Fig. S2). This observation further supports an altered PCP pathway in the *Dlx5;6* DKO model of ectrodactyly.

Cultures of embryonic limbs recapitulate normal and ectrodactyly limb development

We set forth to establish and optimize an *ex vivo* whole-organ culture methods suitable for the embryonic limbs. In a first set of experiments, we collected normal limbs at E11.5 and maintained them in culture for 24 and 48 h, and examined the expression of *Dlx2* and *Fgf8* (well established AER markers) by *in situ* hybridization. We observed a nearly normal expression of *Fgf8* and *Dlx2* mRNAs (Supplementary Material, Fig. S3). We also examined the expression pattern of *Sox9* (a marker of early chondrogenic mesenchymal condensations) in *ex vivo* cultured limbs, by *in situ* hybridization, and found it to be much similar to the normal expression in dissected limbs (Supplementary Material, Fig. S3). Up to 48 h, the culture conditions, we are using are able to maintain the normal organization of the AER and of the skeletogenic territories. Conversely, when the *ex vivo* cultures were setup from *Dlx5;6* DKO limbs, at the same age, we observed signs of ectrodactyly, including the loss of *Dlx2* and *FGF8* expression in the central AER, and abnormal organization of the central chondrogenic elements. Thus, we conclude that these culture conditions are adequate to recapitulate normal limb development and the ectrodactyly phenotype, for a maximum of 48 h.

Addition of Wnt5a to *ex vivo* cultured *Dlx5;6* DKO limbs restores AER identity and function

The altered polarity of the AER cells in *Dlx5;6* DKO limbs, and the reorientation response observed upon addition of Wnt5a on dissociated ectoderm cells, led us to speculated that exposure of *Dlx5;6* DKO whole embryonic limbs to Wnt5a might rescue a normal identity/specialization/activity of the central wedge of the AER. We, therefore, carried out *ex vivo* whole cultures of embryonic hindlimbs from WT and *Dlx5;6* DKO embryos, in the presence or absence of exogenous Wnt5a. The addition of Wnt5a for 24 or 48 h, on cultured *Dlx5;6* DKO limbs resulted in the re-expression of the marker gene *Dlx2*, detected by whole-mount *in situ* hybridization, while no evident effect was observed on normal cultured limbs under the same experimental conditions (Fig. 5A). Thus, we conclude that *Wnt5a* is implicated in the onset of the ectrodactyly phenotype, and its re-expression can revert the dysmorphic phenotype caused by the loss of *Dlx5* and *Dlx6*. Under the same conditions, the addition of FGF8 alone did not exert any evident effect on the *Dlx5;6* DKO limb AER and mesoderm (see below).

To further consolidate this finding, we carried out real-rime qPCR to detect the expression of a set of mRNA, relevant for limb development and/or implicated in non-canonical Wnt signaling, on samples from cultured *Dlx5;6* DKO hindlimbs treated with Wnt5a, or untreated as control. We observed that upon exposure to Wnt5a, the *Dlx* mutant limbs expressed a 2-fold higher levels of *Wnt5a* and *Fgf8* mRNAs, while the level of *Wnt10b* mRNA remained unchanged (Fig. 5B). As control, treatment of WT limbs with Wnt5a did not yield relevant changes in the expression of any of these genes (Fig. 5B).

We, then, examined marker expression and stratification of the AER following exogenous addition of Wnt5a, under the same experimental conditions. Limbs from WT and *Dlx5;6* DKO embryos were cultured for 48 h in the presence (or absence) of Wnt5a, then were sectioned and immunostained with anti-p63 and anti-E-cadherin. Compared with untreated *Dlx5;6* DKO limbs, in which the AER is poorly stratified (14), a significant recovery of the stratification was observed in mutant limbs (five of six limbs examined) upon addition of Wnt5a (Fig. 5C). Furthermore, the level of p63 immunostaining signal, known to be diminished in the AER of *Dlx5;6* DKO limbs (14) was restored to nearly normal level upon the addition of Wnt5a to cultures of mutant hindlimbs (Fig. 5C). These data further confirm the recovery of normal AER morphology and function upon exposure to Wnt5a.

Inhibition of JNK in cultured limbs mimics aspects of AER misfunctions

The phosphorylation of JNK has been implicated as a signal transduction event in the PCP and in non-canonical Wnt5a-dependent pathways (27,32). We hypothesized that in the embryonic limbs Wnt5a may act via phosphorylation of JNK. We treated cultured WT limbs with SP600125, a known inhibitors of JNK and examined the AER by whole-mount *in situ* hybridization to detect the *Dlx2* marker mRNA. As shown in Figure 6A, treatment with all doses of JNKi caused a down-regulation of the *Dlx2* mRNA; with lower doses only the central wedge of the AER was affected.

As control for the specificity of the effect of the inhibitor, *in situ* hybridization was carried out on treated embryos, to detect the *Shh* mRNA (expressed in the proximal-posterior margin of the limb bud and presumed not to be involved in the Dlx5–Dlx6 molecular cascade). The result shows that *Shh* expression was unchanged following treatment with JNKi (Fig. 6B). To consolidate this finding, we determined the abundance of *Wnt5a*, *Fgf8* and *Wnt10b* mRNAs in WT hindlimbs treated with JNKi, by real-time qPCR. We observed that the expression of *Wnt5a* and *Fgf8* mRNAs was significantly diminished, while the level of expression of *Dlx5* and *Wnt10b* mRNA did not change (Fig. 6). These data confirm that Wnt5a acts through JNK/PCP pathway in order to recovery normal AER identity and most probably also the function.

Since Wnt5a is able to reoriented ectodermal cells in mixed primary cultures, we treated mixed primary cultures of ectoderm cells from WT limbs with Wnt5a and the JNK inhibitor, in combination, and examined the cell orientation by GM130 immunostaining (see above). The re-orientation effect of *Wnt5a* was completely abolished in the presence of the inhibitor (Fig. 4), further confirming that Wnt5a acts via the PCP/JNK pathway to polarize ectodermal cells.

Rhou is down-regulated in *Dlx5;6* DKO hindlimbs

Recently, we have shown that the small-GTPase RhoU is transcriptionally induced via a JNK-dependent PCP pathway by both canonical and non-canonical Wnt ligands (47) (and Orecchia *et al.* manuscript in preparation). Rho GTPases are well-known regulators of cytoskeletal organization and dynamics as well as of cell polarity (51). In particular, RhoU was shown to play a role in the control of cell shape and in microvilli formation (52), which are both altered in the *Dlx5;6* DKO AER cells (14) (Supplementary Material, Fig. S2), associated to reduced Wnt5a levels.

Previous experiments indeed detected a significant down-regulation of *RhoU* mRNA in *Dlx5;6* DKO mutant hindlimbs (Fig. 2B), while no difference was observed when comparing WT and *Dlx5;6* DKO forelimbs (not shown). We then examined the level of *RhoU* expression in *Dlx5;6* DKO limbs, maintained *ex vivo*, and exposed to Wnt5a. Treatment of mutant limbs with

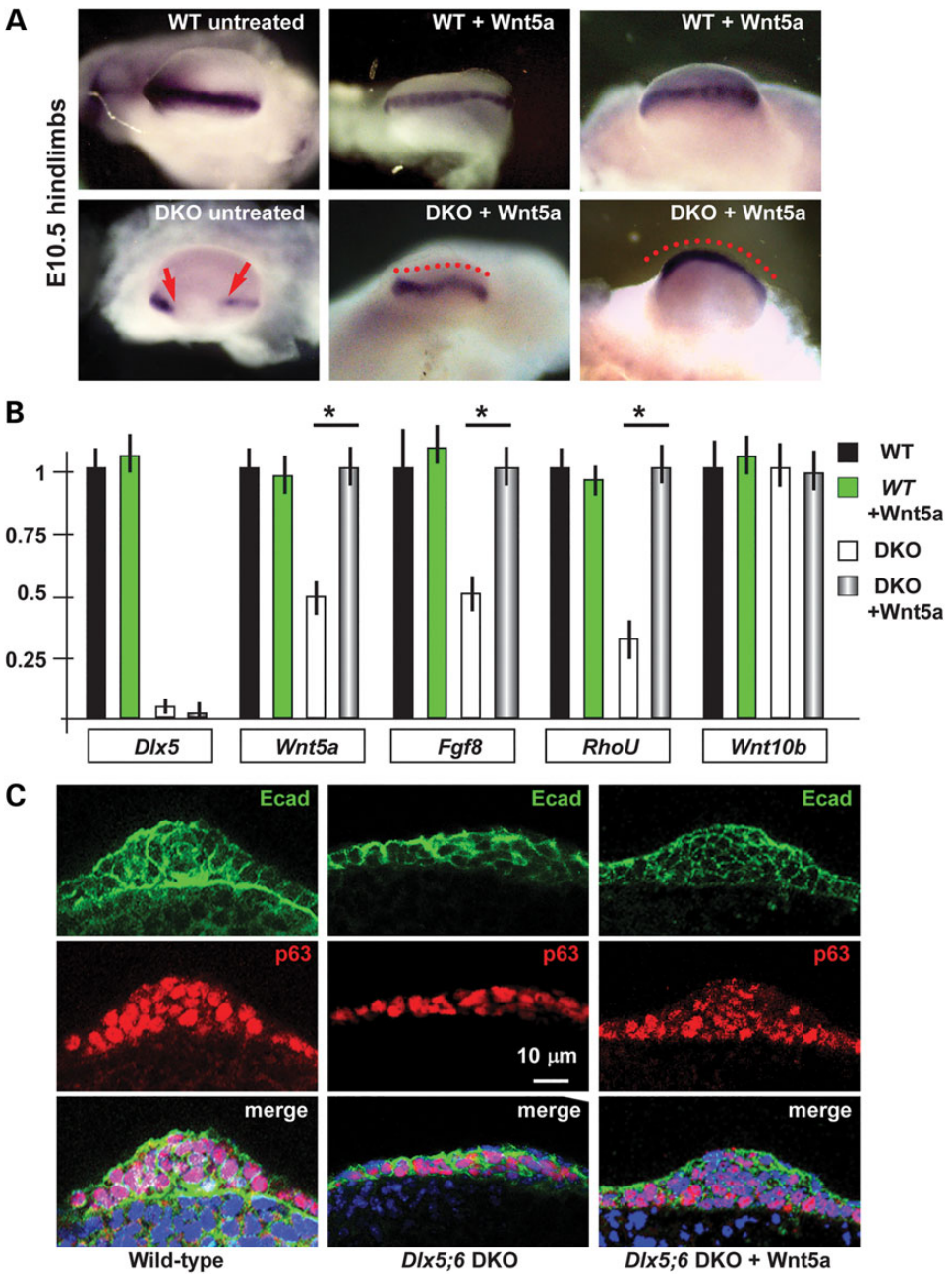

Figure 5. Cultured normal and *Dlx5;6* DKO limbs and their response to Wnt5a. (**A**) Whole-mount *in situ* hybridization to detect *Dlx2* on cultured limbs. Micrographs are taken from the distal side (AER toward the camera). Red-dotted lines indicate the contour of the AER. Red arrows indicate the beginning and the end of a 'no expression' region. (**B**) Real-time qPCR to determine the relative abundance of *Dlx5*, *Wnt5a*, *Fgf8*, *RhoU* and *Wnt10b*, in cultured WT or *Dlx5;6* DKO hindlimbs, either treated with Wnt5a or left untreated. Histogram legend is reported on the right. The expression in the untreated WT limbs is normalized =1. Asterisks indicate the statistical significance. (**C**) Immunofluorescent staining of sections of cultured hindlimbs from WT untreated (left panels) or *Dlx5;6* DKO embryos, either left untreated (middle panels) or treated with Wnt5a (right panels). Staining for E-cadherin (green) and p63 (red) are shown. Bottom panels show the merged signal. While lines indicate the contour of the AER. Scale bars are inserted. The section plane is the same as in Figure 1D.

Wnt5a induced a 2-fold increase in the level of *RhoU* mRNA, and restored the level of the WT (Fig. 5B). Conversely, we examined the abundance of *RhoU* mRNA upon treatment of WT limbs, maintained *ex vivo*, with JNKi. We observed a significant down-regulation of *RhoU* expression upon inhibition of JNK (Fig. 6C). These data suggest that indeed RhoU is a target of the JNK-dependent Wnt5a signal in the hindlimbs AER, and that its expression contributes to the regulation of cell shape during limb development.

FGF8 alone does not rescue expression of AER markers

FGF8 is a key-diffusible molecule expressed by the AER cells (40,42,43), down-regulated in the *Dlx5;6* DKO limbs (11,13). FGF8 has been shown to regulate Pr–Di migration velocity, but not the direction of mesenchymal cells of the limb buds (32). Exploiting *ex vivo* limb cultures, we decided to test the effect of exogenously added FGF8 on *Dlx5;6* DKO limbs. Surprisingly, the results indicate that FGF8 alone is unable to restore expression of AER markers (not shown). To explain this result, we examined the

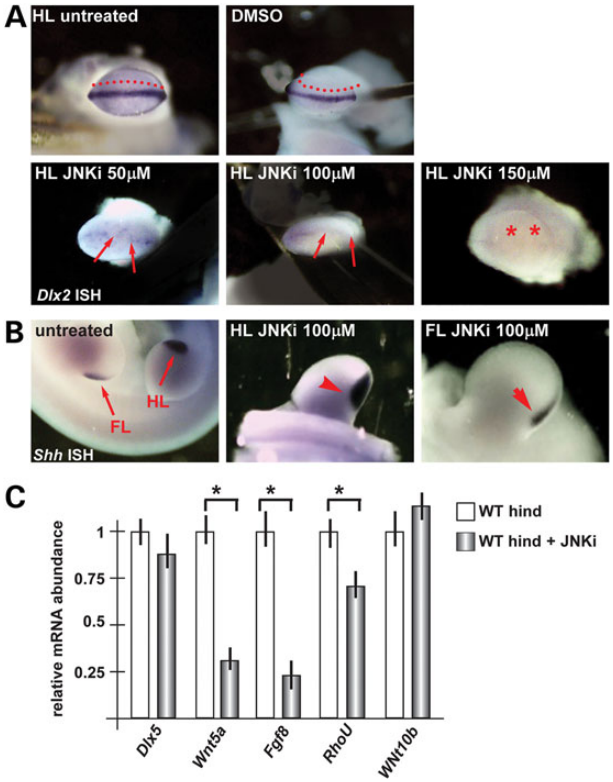

Figure 6. Cultured normal limbs and their response to JNK inhibitor. (**A**) Whole-mount *in situ* hybridization to detect *Dlx2*. Legend as in Figure 5. Red asterisks indicate 'absence of signal'. (**B**) Whole-mount *in situ* hybridization to detect Shh expression as control of no off target effects of JNKi. (**C**) Real-time qPCR to quantify the expression of *Dlx5*, *Wnt5a*, *Fgf8*, *RhoU* and *Wnt10b*, in cultured WT hindlimbs (B) or forelimbs (C). In each case, the limbs were either treated with JNKi (patterned bars) or left untreated (open bars). The expression in the untreated limbs is normalized =1. Asterisks indicate the statistical significance.

expression of *FgfR1*, the main FGF8 receptor in the limb buds, and observed a 40% reduction of *FgfR1* mRNA. As control, we also examined the mRNA level of non-canonical Wnt receptors *Ryk*, *Ror2*, *Fzd3* and *Fzd6*, and of the PCP molecule *Vangl2* (21,23,25,26), but their expression was unaffected in *Dlx5;6* DKO limbs (Supplementary Material, Fig. S4A).

The reduced *FgfR1* expression could result from a direct Dlx5; Dlx6 transcriptional regulation on *FgfR1* expression, as predicted Dlx5-binding sites (37) are present near the promoter region of the *FgfR1* locus (Supplementary Material, Fig. S4B). We carried out chromatin immunoprecipitation (ChIP) experiments on this predicted site, using a myc-tagged versions of WT DLX5 in SH-SY5Y cells, which express *Dlx5* and *FgfR1* mRNAs endogenously. The results indicate that the DLX5 protein occupies the predicted chromatin site (Supplementary Material, Fig. S4C). These results indicate that in the absence of Dlx5 and Dlx6 *FgfR1* expression is down-modulated due to direct transcription regulation, suggesting that responsiveness to FGF8 might be impaired and thus explaining the inability of FGF8 alone to restore AER marker expression in cultured limbs.

Discussion

Here, we show a novel function of the non-canonical Wnt5a signaling molecule for the establishment the polarization of the AER ectodermal cells of the developing limb, essential for their morphogenetic activity. Our data also consent to place the SHFM-causing genes Dlx5 and Dlx6 upstream of Wnt5a, and indicate that restoration of Wnt5a partially reverts AER misorganization and limb dysmorphology.

Wnt5a and limb development

The role of β-catenin-dependent 'canonical' Wnt signaling in limb development and AER formation is well-recognized (53–57). Wnt ligands also activate two β-catenin-independent 'non-canonical' pathways, distinct although intersecting with the canonical one (24,25). Mouse embryos lacking *Wnt5a*, the best known non-canonical Wnt, display specific distal limb phenotypes (19,20), similar although not identical, to the defects seen in embryos lacking the receptors *Ryk* or *Ror2* (21–23). The cellular activity of Wnt5a is linked to the PCP and CE morphogenetic processes described in other species such as Xenopus and zebrafish embryos (58–61). Specifically, recent data indicate that Wnt5a, via PCP, controls the orientation of mesenchymal cell divisions and migration during Pr–Di limb bud elongation (32) and cell shape during condensation of digital cartilages in the mouse embryo (26).

Cell polarity and AER formation

The AER precursors derive from a broad domain of ventrally positioned ectoderm cells, which undergo a CE-type of morphogenetic cell movements (33,34). Once the AER has formed, and given the peculiar position of the AER cells at the Do–Ve margin of the limb bud, it is logical to expect that the AER cells possess a planar polarity in addition to a baso-apical polarity (18,24,25,62,63). This possibility is clearly supported by our immunostaining data on the whole limb bud and on cultured ectodermal cells, in the latter case we show that Wnt5a signaling participates in the establishment of their polarization and orientation. Due to the diffusible nature of Wnt ligands, these effects are likely to be exerted in an paracrine fashion, although an autocrine cell-autonomous effect cannot be excluded.

Defects in polarization and orientation of the perichondral cells are the cellular cause underlying the Synpolydactyly (SPD) disease in which the metacarpals (long bones) are transformed into carpals (cuboid bones) (64). Thus, it is plausible that defects in the AER cells polarization might cause SHFM and related malformations. Indeed, with the present data we are able to place the SHFM-causing genes *Dlx5* and *Dlx6* upstream of *Wnt5a*, and likewise the SPD causing gene *HOXD13* (65) has been proposed to be upstream of *Wnt5a* (64). The defects observed in *Spdh* mice as well as the SHFM *Dlx5/6* DKO mice are accompanied by misregulation of both the β-catenin-dependent and the PCP Wnt pathways. Consistently, we find an increased number and altered position of β-catenin/lacZ positive cells in the *Dlx5;6* DKO limbs. These observations suggest that a local *Hox* code influence cell shape via a local induction of paracrine factors such as Wnt5a.

Mice mutant for the components of PCP *Vangl2*, *Fzd3* or *Fzd6* show limb defects (28), similar to those observed in *Wnt5a* mutant embryos. However, a closer analysis of the limb phenotypes of *Wnt5a* and PCP mutant models has led Lau *et al.* (35) to propose that PCP is not essential for AER formation. Their key argument is that in several PCP-deficient embryos models the AER forms normally. However, the organization of the AER cells following its formation was not examined, thus it is well possible that the PCP plays a role at a slightly later stage, when the AER is formed. To support this possibility, in *Dlx5;6* DKO embryos the AER forms normally but then shows signs of altered cell polarity and

stratification. Since Wnt5a is down-modulated in these mutant limbs, this also indicates that the altered expression of *Wnt5a* is compatible with the formation of a normal AER, but then leads to altered cell polarity and stratification. We propose that the establishment and/or maintenance of a correct basoapical and PCP of the AER cells after AER formation is an essential step requiring *Dlx5* and *Dlx6* gene expression and as normal levels of Wnt5a.

Another set of evidence supporting a role for PCP in AER function derives from the conditional inactivation of *Porcn*, a gene required for the export of Wnt ligands. These models clearly reveal a requirement for both ectoderm- and mesenchymal-derived Wnts for limb development (66), although they do not provide indications on which Wnt is specifically implicated in each territory. Thus, an involvement of ectodermal Wnt5a for the AER function and maintenance, if not its formation, is plausible but so far has remained poorly explored.

Finally, a recent observation changes the view on the involvement of PCP in AER formation. According to Lau *et al.* (35), both mesenchymal and ectodermal forces generate stress patterns that contribute to AER formation, without the involvement of PCP. In our study, we have excluded evident changes in proliferation and apoptosis of the mesenchymal cells of Dlx5;6 DKO limbs, that might cause abnormal stretch forces, and the AER forms normally. Instead, at later stages after AER formation, e.g. when the AER has acquired stratification, in *Dlx5;6* DKO limbs the planar polarity of AER cells is affected, and some of the PCP pathway molecules are implicated in this defect. We conclude that PCP might not be implicated in AER formation, but appears to be required for subsequent polarity and stratification of the AER cells, hence for its function.

Components of non-canonical WNT signaling in human limb malformations

In human, *WNT5A* and the PCP receptor Ror2 (67) have been linked to the Robinow syndrome (OMIM 180700) (OMIM 268310), characterized by mesomelic limb shortening (68–71). *ROR2* mutations have also been associated to brachydactyly type B1 (OMIM 113000), another congenital distal limb malformation. The present data, combined with other data (32), point to the interesting possibility to deeply examine *Ror2*$^{-/-}$ mice (26), and further investigate on the role of non-canonical Wnt signalling on the control of cell shape and polarity, and the limb defects phenotype caused by its alteration.

AER restoration

In the present study, we show that *ex vivo* administration of Wnt5a to cultured limbs partially reverts AER misorganization and dysmorphology. The suitability of the *ex vivo* limb culture approach has been well-established (72–75). Even though this represents an 'artificial' model system, it is currently the model that most closely resembles *in vivo* development and recapitulates most features. Indeed, cultured limbs have been shown to maintain cell and tissue morphology, Pr–Di elongation (76), interdigital web formation (77), expression of key molecular markers and signaling interactions. We demonstrated the feasibility of this technique analyzing the normal expression of specific AER markers *Fgf8* and *Dlx2* as well as *Shh* in the zone of polarizing activity. A comprehensive analysis of gene expressed in cultured limbs compared with *in vivo* limbs, as well as limbs treated with Wnt5a compared with untreated ones, by omic analyses might be informative.

Materials and Methods

Mouse strains

All procedures using mice were approved by the Ethical Committee of the University of Torino, and by the Italian Ministry of Health. Mice DKO for *Dlx5* and *Dlx6* (named *Dlx5;6* DKO) have been previously reported by us (12) and other authors (11); these mice display ectrodactyly of the hindlimbs. The heterozygous animals were viable and showed no obvious skeletal malformation. Therefore, we considered the +/+ and +/– embryos 'normal', unless otherwise specified. *Dlx5;6* DKO embryos were recognized by morphological examination of the head (12,78). For confirmation, genotypes were done by PCR amplification. Transgenic mice containing the *LacZ* reporter sequence linked to a Wnt-β-catenin response element (named BAT-LacZ) were provided by Dr S. Piccolo (University of Padova) (49). These animals were viable and fertile, and were maintained as a heterozygous strain. Crossbreeding of *Dlx5;6* heterozygotes with BAT-*LacZ* mice yielded double heterozygous individual at approximately the expected frequency (25%).

Whole-mount and section *in situ* hybridization

In situ hybridization was carried out with DIG-labeled probes corresponding to the antisense sequence of the following murine cDNA fragments: *Dlx5*, a 750 bp fragment spanning the entire coding sequence; *Dlx6*, a 350 bp fragment spanning the third and part of the fourth (non-coding) exons (79). The probe for *Dlx2* was from Dr Antonio Simeone (Naples, Italy) (80). The probe for *Shh* was previously described (81). The probe for *Sox9* is a 500 bp fragment in the 3′ of the *Sox9* cDNA, sequence verified. Probes for *Wnt5a*, *Wnt5b*, were obtained from A. McMahon (Harvard University, USA). The hybridization signal obtained with these probes was consistent with published data. For each probe, at least two normal and three mutant specimens were examined.

For whole-mount hybridization the procedure described in Wilkinson *et al.* (1992) was used. For section hybridization, hindlimbs from E10.5–E12.5 embryos were fixed in 4% paraformaldehyde (PFA) ON, rinsed in phosphate-buffered saline (PBS), cryoprotected with 20% sucrose, frozen and sectioned. Serial cryostatic sections (11 μm thick) were collected on RNase-free glass slides and processed as described (82). Briefly, sections were post-fixed in 4% PFA for 5 min, rinsed in 0.1 M PBS and treated with proteinase K 3 μg/ml. Tissues were then refixed in 4% PFA for 5 min, washed in PBS and deacetylated in 1.35% triethanolamine, 0.02N HCl, 0.25% acetic anhydrate (pH8) for 10 min at RT. Subsequently, sections were incubated in PBS-1% Triton X-100 for 30 min, rinsed in PBS and covered with hybridization solution (50% formamide, 5× SSC, 5× Denhart's solution, 250 μg/ml yeast tRNA, 500 μg/ml shared salmon sperm DNA) for 2 h at RT. Hybridization occurred overnight at 60°C in a humidified chamber. Following hybridization, slides were rinsed in 0.2× SSC at 60°C for 1 h, then in 0.2× SSC for 5 min and finally in B1 (0.1 M Tris, pH 7.5, 0.15 M NaCl) for 5 min at RT. Sections were blocked for 1 h in 10% normal goat serum in B1 at RT and then incubated overnight at 4°C with an anti-DIG-AP conjugate antibody (Roche) in B1. Next, slices were rinsed in B1 several times, incubated 5 min at RT in B3 buffer (0.1 M Tris, pH 9.5, 0.1 M NaCl, 50 mM $MgCl_2$, 0.1% Tween-20, 0.24 mg/ml levamisole) and the signal was revealed with BM-Purple substrate (Roche).

Immunostaining on embryonic limbs and embryonic ectoderm cells

Embryonic limbs were dissected in PBS, collected in 4% PFA and fixed for 12–16 h depending on the age, washed in PBS and

cryoprotected. Cryostatic sections (12–15 μm thick) were collected on glass slides, blocked with 1% bovine serum albumin (BSA) in PBS for 1 h at RT and incubated with the following primary antibodies, diluted from 1:250 to 1:50 in 1% BSA in PBS, ON at 4°C: anti-GM130 (BD), with anti-p63 (4A4 sc-8431, Santa Cruz), anti ZO-1 (InVitrogen) and with anti-E-cadherin (36/E 610182, BD). Sections were rinsed with PBS and incubated with secondary antibodies anti-mouse-Cy2 and anti-rabbit-Cy3 (Jackson ImmunoResearch) diluted 1:200, 1 h at RT, rinsed in PBS, counterstained with DAPI and examined with a Zeiss Observer-Z1 fluorescent microscope, equipped with the Apotome system.

For a semi-quantitative assessment of the orientation of the AER cells in whole-limbs, the results were visualized using the Rose2.0 software, showing the angle of each cell's longest axis as a unidirectional rosette graph divided into Bins of 15°. Each interval represents 25 cells per Bin. A minimum of $N = 150$ AER cells were counted for each of the two genotypes.

Proliferation and apoptosis in the limb bud

Proliferation was determined by BrdU incorporation at embryonic time from E11 to E12.5. BrdU was injected intraperitoneally (100 μg/g of body weight), 6 h later the animals were sacrificed, embryos were fixed and processed for *in situ* hybridization, the limb buds were cryo-sectioned parallel to the Do–Ve plane, to better visualize the AER and the underlying PZ mesenchyme. Sections stained with monoclonal anti-BrdU (Serotech, used 1:200) were examined by conventional microscopy, positive nuclei in the AER were scored, at least 200 cells were examined, results were expressed as the fraction of BrdU+ nuclei over the estimated total number of nuclei counted (at least 200).

Detection of Wnt-β-catenin responsive cells in the AER

To visualize the cells in which the *Wnt* pathway is active at a given time during development, we used the BAT-*lacZ* reporter mice (49). These utilize the *lacZ* reporter under control of an artificial promoter containing seven copies of the canonical TCF/LEF DNA-binding sites and a minimal promoter-TATA box. Relevant to this study, reporter expression is found in all structures the mouse embryo outgrowing from the main body axis (ear pinnae, branchial arches, genital and limb primordia). This distribution is remarkably similar to the expression of *Dlx* genes (12,83). In particular, in the developing limb buds, expression of the *lacZ* reporter appears in the AER starting at E9.5 of the mouse embryo, confirming the notion that *Wnt* signaling and β-catenin activation is required for AER induction and maintenance. To examine Wnt-β-catenin signaling in the AER of the *Dlx5;6* DKO limbs, BAT-*lacZ* mice (see above) were cross-bred with *Dlx5;6* heterozygous mice to generate double heterozygous ones, obtained at the expected frequency (25%). From the inter-breeding of these, *Dlx5;6* DKO;BAT-*lacZ* embryos were obtained at the expected frequency (12.5%). Embryos were collected at the ages E10.5 and E11.5, fixed in 4% PFA for 30′ at RT, washed in PBS and stained in whole-mount ON at 32°, as described (12).

Cultures of whole embryonic limbs

Isolated mouse embryonic trunk fragments were cultured essentially using established procedures (72,75,77) with minor modifications (84). This culturing method enables *in vitro* development of mouse embryonic limb buds for up to 48 h. Most importantly, the molecular alterations observed in *Dlx5/6 DKO* limb buds are maintained during culturing. Briefly, WT or *Dlx5/6 DKO* mouse embryos at the age E11.5 were dissected to remove the head and the organs, keeping the two forelimbs or the two hindlimbs attached to the trunk, and maintained in serum-free, high-glucose Dulbecco's modified Eagle's medium (DMEM) (GIBCO-InVitrogen), supplemented with penicillin/streptomycin, L-glutamine, non-essential amino acids, sodium pyruvate, D-glucose, L-ascorbic acid, lactic acid, d-biotin, vitamin B12 and para-aminobenzoic acid. The embryo parts were mounted on an inverted V-shaped metal grid, pinned in a horizontal position with the limbs floating at the air–liquid interface. The cultures were then maintained for a maximum of 48 h in 8% CO_2 at 37°C. Wnt5a, FGF8 or the JNK inhibitor SP600125 (Sigma-Aldrich, Saint Louis, MO, USA) were added to the medium just prior to mounting. Purified recombinant Wnt5a or FGF8 (R&D system) were used either alone or in combination, at the final concentration of 1 μg/ml each. The JNK inhibitor was used at the final concentration of 50–150 μM. After culture, the tissues were rapidly washed with PBS, fixed with 4% PFA for 6–8 h and included or used for whole-mount *in situ* hybridization. Only trunks with normally developed limb buds (significant growth and no malformation or AER damage) were then included in the analysis. At least 5–10 grafted limb buds from three or more independent experiments were analyzed and yielded identical results.

Primary cultures of embryonic ectoderm and mesenchyme

A minimum of 10 hindlimbs were rapidly collected from E11 WT embryos, the tissues were briefly treated with Accutase (Sigma) for 10 min at 37°, and then mechanically dissociated into a near single-cell suspension by passing thought a plastic pipette, at least 20 times. Cells were collected by centrifugation at 1000 rpm for 2′ and resuspended in DMEM supplemented with 10% FBS. Cells were then plated on laminin-coated 35 mm plastic dishes, at density 10^4 cells/ml, and incubated in the medium indicated above for whole-limb culture. To verify the presence of ectoderm cells, the dishes were immunostained with anti-E-cadherin and anti-p63 antibodies, revealing the presence of well-defined clumps of E-cadherin+;p63+ epithelial cells, surrounded by E-cadherin−;p63− embryo fibroblasts. Agarose drops containing ~10^5 COS7 cells, either transfected with *Wnt5a*-expression vectors or with the same empty vector as control, were prepared according to established procedures, placed asymmetrically in the dish and maintained for 48 h. Dishes were then fixed in PFA 2%, washed with PBS and used for immunostaining. For the detection of cell orientation the same conditions as for limb cryostatic sections were used (above). Nuclei were counterstained with DAPI. Micrographs were taken keeping track of the position of the agarose drop. To assess cell orientation, we kept track of the position of the Wnt5a-expressing cell pellet, and determined the orientation of the Golgi (GP130+) versus the nucleus, and the orientation of the basal body/centrosome versus the nucleus, of a minimum of $N = 200$ p63+ cells for each genotype and/or condition. The quantification was done using ImageJ for the quantification of the angle between the Pr–Di axis of the limb bud or the direction of the drops placed in the well and the cell axis.

Image analysis

Immunostained sections were examined using a Leica TSCII SP5X confocal microscope. Multitrack analysis was used for image acquisition. Raw images were digitally processed to normalize the background and optimize the contrast, with

Photoshop (Adobe), and mounted with QuarkXpress (Pantone). Semi-quantitative immunofluorescence analysis for p63 was performed with the ImageJ-64 (v1.45) software. Images were first converted to grayscale, and the DAPI channel was used to count nuclei. p63 intensity was quantified after background correction and normalized respect to the number of nuclei in the region of interest. Data are presented as mean and SD of ~4/5 sections from three different embryos. A significant *T*-test score is indicated by asterisks: $^{*}P<0.05$ and $^{**}P < 0.01$.

Real-time qPCR for quantification of mRNAs in limb buds

For the analysis of *Dlx5* and *Dlx6* target genes, E11.25 anterior or posterior limb buds (6 WT and six mutants, two independent experiments) were dissected, pooled in Trizol Reagent (Roche) and extracted as indicated by the manufacturer. For the analysis of expression along the length of the AER, a minimum of 10 limbs from E11.25 embryos were individually dissected in three sectors, anterior, medial, posterior (A, M, P, respectively) under stereomicroscope examination, using fine needles and scissors, as detailed in the figure. Sectors were then pooled and collected in Trizol Reagent. RNA quality, primer efficiency and correct product size were verified by real-time PCR and agarose gel electrophoresis. Real-time qPCR was performed with LightCycler (Roche) using FastStart DNA MasterPLUS SYBR-Green I (Roche). Five microliters of cDNA were used in each reaction. All samples were done in triplicates. The specificity and absence of primer dimers was controlled by denaturation curves; for each mRNA examined only one denaturation peak was observed. GAPDH was used for normalization, calculated using LightCycler Software 3.5.3. Primer sequences are reported in Supplementary Material, Table SI.

ChIP was done on the chromatin of *DLX5-myc* transfected SH-SY5Y neuroblastoma cells, using anti-myc antibody, as published (85). The primers used to detect the DLX5-binding element near the *FgfR1* locus are reported in Supplementary Material, Table SI.

Supplementary Material

Supplementary Material is available at *HMG* online.

Acknowledgements

We thank Dr A. McMachon (Harvard University Cambridge, MA, USA) for the generous gift of *Wnt* probes. We thank Drs Luisa Guerrini (University of Milano), Enzo Calautti and Massimo Santoro (University of Torino) for their helpful criticism on the manuscript.

Conflict of Interest statement. None declared.

Funding

G.R.M. is supported by a grant from Italian Telethon Foundation (GGP11097) and from Fondazione C.R.T. (contributo 2014-2015). V.P. is supported by the Italian Cancer Research Association (AIRC IG13009), the Italian Ministry of University and Research (MIUR PRIN), the Compagnia San Paolo (Ateneo/SanPaolo) and the Truus and Gerrit van Riemsdijk Foundation, Liechtenstein (donation). Funding to pay the Open Access publication charges for this article was provided by the Italian Telethon Foundation.

References

1. Gurrieri, F. and Everman, D.B. (2013) Clinical, genetic, and molecular aspects of split-hand/foot malformation: an update. *Am. J. Med. Genet. A.*, **161A**, 2860–2872.
2. Sowinska-Seidler, A., Socha, M. and Jamsheer, A. (2013) Split-hand/foot malformation—molecular cause and implications in genetic counseling. *J. Appl. Genet.*, **55**, 105–115.
3. Aziz, A., Irfanullah, , Khan, S., Zimri, F.K., Muhammad, N., Rashid, S. and Ahmad, W. (2013) Novel homozygous mutations in the WNT10B gene underlying autosomal recessive split hand/foot malformation in three consanguineous families. *Gene*, **534**, 7.
4. Conte, D., Guerrini, L. and Merlo, G.R. (2015) Novel Cellular and Molecular Interactions During Limb Development, Revealed from Studies on the Split Hand Foot Congenital Malformation, New Discoveries in Embryology, InTech.
5. Guerrini, L., Costanzo, A. and Merlo, G.R. (2011) A symphony of regulations centered on p63 to control development of ectoderm-derived structures. *J. Biomed. Biotechnol.*, **2011**, 864904.
6. Shamseldin, H.E., Faden, M.A., Alashram, W. and Alkuraya, F.S. (2012) Identification of a novel DLX5 mutation in a family with autosomal recessive split hand and foot malformation. *J. Med. Genet.*, **49**, 16–20.
7. Koster, M.I. (2010) p63 in skin development and ectodermal dysplasias. *J. Invest. Dermatol.*, **130**, 2352–2358.
8. Khan, S., Basit, S., Zimri, F.K., Ali, N., Ali, G., Ansar, M. and Ahmad, W. (2012) A novel homozygous missense mutation in WNT10B in familial split-hand/foot malformation. *Clin. Genet.*, **82**, 48–55.
9. Ugur, S.A. and Tolun, A. (2008) Homozygous WNT10b mutation and complex inheritance in split-hand/foot malformation. *Hum. Mol. Genet.*, **17**, 2644–2653.
10. Blattner, A., Huber, A.R. and Rothlisberger, B. (2012) Homozygous nonsense mutation in WNT10B and sporadic split-hand/foot malformation (SHFM) with autosomal recessive inheritance. *Am. J. Med. Genet. A.*, **152A**, 2053–2056.
11. Robledo, R.F., Rajan, L., Li, X. and Lufkin, T. (2002) The Dlx5 and Dlx6 homeobox genes are essential for craniofacial, axial, and appendicular skeletal development. *Genes Dev.*, **16**, 1089–1101.
12. Merlo, G.R., Paleari, L., Mantero, S., Genova, F., Beverdam, A., Palmisano, G.L., Barbieri, O. and Levi, G. (2002) Mouse model of split hand/foot malformation type I. *Genesis*, **33**, 97–101.
13. Lo Iacono, N., Mantero, S., Chiarelli, A., Garcia, E., Mills, A.A., Morasso, M.I., Costanzo, A., Levi, G., Guerrini, L. and Merlo, G.R. (2008) Regulation of Dlx5 and Dlx6 gene expression by p63 is involved in EEC and SHFM congenital limb defects. *Development*, **135**, 1377–1388.
14. Restelli, M., Lopardo, T., Lo Iacono, N., Garaffo, G., Conte, D., Rustighi, A., Napoli, M., Del Sal, G., Perez-Morga, D., Costanzo, A. *et al.* (2014) DLX5, FGF8 and the Pin1 isomerase control DeltaNp63alpha protein stability during limb development: a regulatory loop at the basis of the SHFM and EEC congenital malformations. *Hum. Mol. Genet.*, **23**, 3830–3842.
15. Restelli, M., Molinari, E., Marinari, B., Conte, D., Gnesutta, N., Costanzo, A., Merlo, G.R. and Guerrini, L. (2015) FGF8, c-Abl and p300 participate in a pathway that controls stability and function of the DeltaNp63alpha protein. *Hum. Mol. Genet.*, **24**, 4185–4197.
16. Panganiban, G. (2000) Distal-less function during Drosophila appendage and sense organ development. *Dev. Dyn.*, **218**, 554–562.
17. Panganiban, G. and Rubenstein, J.L. (2002) Developmental functions of the Distal-less/Dlx homeobox genes. *Development*, **129**, 4371–4386.
18. Eisenberg, L.M., Ingham, P.W. and Brown, A.M. (1992) Cloning and characterization of a novel Drosophila Wnt gene,

Dwnt-5, a putative downstream target of the homeobox gene distal-less. *Dev. Biol.*, **154**, 73–83.
19. Yamaguchi, T.P., Bradley, A., McMahon, A.P. and Jones, S. (1999) A Wnt5a pathway underlies outgrowth of multiple structures in the vertebrate embryo. *Development*, **126**, 1211–1223.
20. Topol, L., Jiang, X., Choi, H., Garrett-Beal, L., Carolan, P.J. and Yang, Y. (2003) Wnt-5a inhibits the canonical Wnt pathway by promoting GSK-3-independent beta-catenin degradation. *J. Cell Biol.*, **162**, 899–908.
21. Andre, P., Wang, Q., Wang, N., Gao, B., Schilit, A., Halford, M.M., Stacker, S.A., Zhang, X. and Yang, Y. (2012) The Wnt coreceptor Ryk regulates Wnt/planar cell polarity by modulating the degradation of the core planar cell polarity component Vangl2. *J. Biol. Chem.*, **287**, 44518–44525.
22. Halford, M.M., Armes, J., Buchert, M., Meskenaite, V., Grail, D., Hibbs, M.L., Wilks, A.F., Farlie, P.G., Newgreen, D.F., Hovens, C.M. *et al.* (2000) Ryk-deficient mice exhibit craniofacial defects associated with perturbed Eph receptor crosstalk. *Nat. Genet.*, **25**, 414–418.
23. Ho, H.Y., Susman, M.W., Bikoff, J.B., Ryu, Y.K., Jonas, A.M., Hu, L., Kuruvilla, R. and Greenberg, M.E. (2012) Wnt5a-Ror-Dishevelled signaling constitutes a core developmental pathway that controls tissue morphogenesis. *Proc. Natl Acad. Sci. USA*, **109**, 4044–4051.
24. Rao, T.P. and Kuhl, M. (2010) An updated overview on Wnt signaling pathways: a prelude for more. *Circ. Res.*, **106**, 1798–1806.
25. van Amerongen, R. and Nusse, R. (2009) Towards an integrated view of Wnt signaling in development. *Development*, **136**, 3205–3214.
26. Gao, B., Song, H., Bishop, K., Elliot, G., Garrett, L., English, M.A., Andre, P., Robinson, J., Sood, R., Minami, Y. *et al.* (2011) Wnt signaling gradients establish planar cell polarity by inducing Vangl2 phosphorylation through Ror2. *Dev. Cell*, **20**, 163–176.
27. Sokol, S.Y. (2015) Spatial and temporal aspects of Wnt signaling and planar cell polarity during vertebrate embryonic development. *Semin. Cell Dev. Biol.*, **42**, 78–85.
28. Wang, B., Sinha, T., Jiao, K., Serra, R. and Wang, J. (2011) Disruption of PCP signaling causes limb morphogenesis and skeletal defects and may underlie Robinow syndrome and brachydactyly type B. *Hum. Mol. Genet.*, **20**, 271–285.
29. Saburi, S., Hester, I., Fischer, E., Pontoglio, M., Eremina, V., Gessler, M., Quaggin, S.E., Harrison, R., Mount, R. and McNeill, H. (2008) Loss of Fat4 disrupts PCP signaling and oriented cell division and leads to cystic kidney disease. *Nat. Genet.*, **40**, 1010–1015.
30. Wang, J., Hamblet, N.S., Mark, S., Dickinson, M.E., Brinkman, B.C., Segil, N., Fraser, S.E., Chen, P., Wallingford, J.B. and Wynshaw-Boris, A. (2006) Dishevelled genes mediate a conserved mammalian PCP pathway to regulate convergent extension during neurulation. *Development*, **133**, 1767–1778.
31. Yang, Y. (2003) Wnts and wing: Wnt signaling in vertebrate limb development and musculoskeletal morphogenesis. *Birth Defects Res. C. Embryo Today*, **69**, 305–317.
32. Gros, J., Hu, J.K., Vinegoni, C., Feruglio, P.F., Weissleder, R. and Tabin, C.J. (2010) WNT5A/JNK and FGF/MAPK pathways regulate the cellular events shaping the vertebrate limb bud. *Curr. Biol.*, **20**, 1993–2002.
33. Altabef, M. and Tickle, C. (2002) Initiation of dorso-ventral axis during chick limb development. *Mech. Dev.*, **116**, 19–27.
34. Guo, Q., Loomis, C. and Joyner, A.L. (2003) Fate map of mouse ventral limb ectoderm and the apical ectodermal ridge. *Dev. Biol.*, **264**, 166–178.
35. Lau, K., Tao, H., Liu, H., Wen, J., Sturgeon, K., Sorfazlian, N., Lazic, S., Burrows, J.T., Wong, M.D., Li, D. *et al.* (2015) Anisotropic stress orients remodelling of mammalian limb bud ectoderm. *Nat. Cell Biol.*, **17**, 569–579.
36. Paina, S., Garzotto, D., Demarchis, S., Marino, M., Moiana, A., Conti, L., Cattaneo, E., Perera, M., Corte, G., Calautti, E. *et al.* (2011) Wnt5a is a transcriptional target of dlx homeogenes and promotes differentiation of interneuron progenitors in vitro and in vivo. *J. Neurosci.*, **31**, 2675–2687.
37. Vieux-Rochas, M., Bouhali, K., Mantero, S., Garaffo, G., Provero, P., Astigiano, S., Barbieri, O., Caratozzolo, M.F., Tullo, A., Guerrini, L. *et al.* (2013) BMP-mediated functional cooperation between Dlx5;Dlx6 and Msx1;Msx2 during mammalian limb development. *PLoS One*, **8**, e51700.
38. Romano, R.A., Smalley, K., Magraw, C., Serna, V.A., Kurita, T., Raghavan, S. and Sinha, S. (2012) DeltaNp63 knockout mice reveal its indispensable role as a master regulator of epithelial development and differentiation. *Development*, **139**, 772–782.
39. Akiyama, H., Chaboissier, M.C., Martin, J.F., Schedl, A. and de Crombrugghe, B. (2002) The transcription factor Sox9 has essential roles in successive steps of the chondrocyte differentiation pathway and is required for expression of Sox5 and Sox6. *Genes Dev.*, **16**, 2813–2828.
40. Boulet, A.M., Moon, A.M., Arenkiel, B.R. and Capecchi, M.R. (2004) The roles of Fgf4 and Fgf8 in limb bud initiation and outgrowth. *Dev. Biol.*, **273**, 361–372.
41. Crossley, P.H., Minowada, G., MacArthur, C.A. and Martin, G.R. (1996) Roles for FGF8 in the induction, initiation, and maintenance of chick limb development. *Cell*, **84**, 127–136.
42. Lewandoski, M., Sun, X. and Martin, G.R. (2000) Fgf8 signalling from the AER is essential for normal limb development. *Nat. Genet.*, **26**, 460–463.
43. Moon, A.M. and Capecchi, M.R. (2000) Fgf8 is required for outgrowth and patterning of the limbs. *Nat. Genet.*, **26**, 455–459.
44. Fallon, J.F. and Saunders, J.W. Jr (1968) In vitro analysis of the control of cell death in a zone of prospective necrosis from the chick wing bud. *Dev. Biol.*, **18**, 553–570.
45. Campbell, G. and Tomlinson, A. (1998) The roles of the homeobox genes aristaless and Distal-less in patterning the legs and wings of *Drosophila*. *Development*, **125**, 4483–4493.
46. Dong, P.D., Chu, J. and Panganiban, G. (2000) Coexpression of the homeobox genes Distal-less and homothorax determines *Drosophila* antennal identity. *Development*, **127**, 209–216.
47. Schiavone, D., Dewilde, S., Vallania, F., Turkson, J., Di Cunto, F. and Poli, V. (2009) The RhoU/Wrch1 Rho GTPase gene is a common transcriptional target of both the gp130/STAT3 and Wnt-1 pathways. *Biochem. J.*, **421**, 283–292.
48. Mikels, A.J. and Nusse, R. (2006) Purified Wnt5a protein activates or inhibits beta-catenin-TCF signaling depending on receptor context. *PLoS Biol.*, **4**, e115.
49. Maretto, S., Cordenonsi, M., Dupont, S., Braghetta, P., Broccoli, V., Hassan, A.B., Volpin, D., Bressan, G.M. and Piccolo, S. (2003) Mapping Wnt/beta-catenin signaling during mouse development and in colorectal tumors. *Proc. Natl Acad. Sci. USA*, **100**, 3299–3304.
50. Krieg, M., Arboleda-Estudillo, Y., Puech, P.H., Kafer, J., Graner, F., Muller, D.J. and Heisenberg, C.P. (2008) Tensile forces govern germ-layer organization in zebrafish. *Nat. Cell Biol.*, **10**, 429–436.
51. Schlessinger, K., Hall, A. and Tolwinski, N. (2009) Wnt signaling pathways meet Rho GTPases. *Genes Dev.*, **23**, 265–277.
52. Loebel, D.A., Studdert, J.B., Power, M., Radziewic, T., Jones, V., Coultas, L., Jackson, Y., Rao, R.S., Steiner, K., Fossat, N. *et al.*

(2011) Rhou maintains the epithelial architecture and facilitates differentiation of the foregut endoderm. *Development*, **138**, 4511–4522.
53. Church, V.L. and Francis-West, P. (2002) Wnt signalling during limb development. *Int. J. Dev. Biol.*, **46**, 927–936.
54. Kawakami, Y., Capdevila, J., Buscher, D., Itoh, T., Rodriguez Esteban, C. and Izpisua Belmonte, J.C. (2001) WNT signals control FGF-dependent limb initiation and AER induction in the chick embryo. *Cell*, **104**, 891–900.
55. McQueeney, K., Soufer, R. and Dealy, C.N. (2002) Beta-catenin-dependent Wnt signaling in apical ectodermal ridge induction and FGF8 expression in normal and limbless mutant chick limbs. *Dev. Growth Differ.*, **44**, 315–325.
56. Galceran, J., Farinas, I., Depew, M.J., Clevers, H. and Grosschedl, R. (1999) Wnt3a-/-like phenotype and limb deficiency in Lef1(-/-)Tcf1(-/-) mice. *Genes Dev.*, **13**, 709–717.
57. Barrow, J.R., Thomas, K.R., Boussadia-Zahui, O., Moore, R., Kemler, R., Capecchi, M.R. and McMahon, A.P. (2003) Ectodermal Wnt3/beta-catenin signaling is required for the establishment and maintenance of the apical ectodermal ridge. *Genes Dev.*, **17**, 394–409.
58. Gong, Y., Mo, C. and Fraser, S.E. (2004) Planar cell polarity signalling controls cell division orientation during zebrafish gastrulation. *Nature*, **430**, 689–693.
59. Heisenberg, C.P., Tada, M., Rauch, G.J., Saude, L., Concha, M.L., Geisler, R., Stemple, D.L., Smith, J.C. and Wilson, S.W. (2000) Silberblick/Wnt11 mediates convergent extension movements during zebrafish gastrulation. *Nature*, **405**, 76–81.
60. Jessen, J.R., Topczewski, J., Bingham, S., Sepich, D.S., Marlow, F., Chandrasekhar, A. and Solnica-Krezel, L. (2002) Zebrafish trilobite identifies new roles for Strabismus in gastrulation and neuronal movements. *Nat. Cell Biol.*, **4**, 610–615.
61. Yin, C., Kiskowski, M., Pouille, P.A., Farge, E. and Solnica-Krezel, L. (2008) Cooperation of polarized cell intercalations drives convergence and extension of presomitic mesoderm during zebrafish gastrulation. *J. Cell Biol.*, **180**, 221–232.
62. Simons, M. and Mlodzik, M. (2008) Planar cell polarity signaling: from fly development to human disease. *Annu. Rev. Genet.*, **42**, 517–540.
63. Zallen, J.A. (2007) Planar polarity and tissue morphogenesis. *Cell*, **129**, 1051–1063.
64. Kuss, P., Kraft, K., Stumm, J., Ibrahim, D., Vallecillo-Garcia, P., Mundlos, S. and Stricker, S. (2014) Regulation of cell polarity in the cartilage growth plate and perichondrium of metacarpal elements by HOXD13 and WNT5A. *Dev. Biol.*, **385**, 83–93.
65. Muragaki, Y., Mundlos, S., Upton, J. and Olsen, B.R. (1996) Altered growth and branching patterns in synpolydactyly caused by mutations in HOXD13. *Science*, **272**, 548–551.
66. Barrott, J.J., Cash, G.M., Smith, A.P., Barrow, J.R. and Murtaugh, L.C. (2011) Deletion of mouse Porcn blocks Wnt ligand secretion and reveals an ectodermal etiology of human focal dermal hypoplasia/Goltz syndrome. *Proc. Natl Acad. Sci. USA*, **108**, 12752–12757.
67. Mikels, A., Minami, Y. and Nusse, R. (2009) Ror2 receptor requires tyrosine kinase activity to mediate Wnt5A signaling. *J. Biol. Chem.*, **284**, 30167–30176.
68. Robinow, M., Silverman, F.N. and Smith, H.D. (1969) A newly recognized dwarfing syndrome. *Am. J. Dis. Child*, **117**, 645–651.
69. Wadia, R.S. (1979) Covesdem syndrome. *J. Med. Genet.*, **16**, 162.
70. Wadia, R.S., Shirole, D.B. and Dikshit, M.S. (1978) Recessively inherited costovertebral segmentation defect with mesomelia and peculiar facies (Covesdem syndrome): a new genetic entity? *J. Med. Genet.*, **15**, 123–127.
71. Wadlington, W.B., Tucker, V.L. and Schimke, R.N. (1973) Mesomelic dwarfism with hemivertebrae and small genitalia (the Robinow syndrome). *Am. J. Dis. Child*, **126**, 202–205.
72. Kuhlman, J. and Niswander, L. (1997) Limb deformity proteins: role in mesodermal induction of the apical ectodermal ridge. *Development*, **124**, 133–139.
73. Michos, O., Panman, L., Vintersten, K., Beier, K., Zeller, R. and Zuniga, A. (2004) Gremlin-mediated BMP antagonism induces the epithelial-mesenchymal feedback signaling controlling metanephric kidney and limb organogenesis. *Development*, **131**, 3401–3410.
74. Panman, L., Galli, A., Lagarde, N., Michos, O., Soete, G., Zuniga, A. and Zeller, R. (2006) Differential regulation of gene expression in the digit forming area of the mouse limb bud by SHH and gremlin 1/FGF-mediated epithelial-mesenchymal signalling. *Development*, **133**, 3419–3428.
75. Zuniga, A., Haramis, A.P., McMahon, A.P. and Zeller, R. (1999) Signal relay by BMP antagonism controls the SHH/FGF4 feedback loop in vertebrate limb buds. *Nature*, **401**, 598–602.
76. Niswander, L., Tickle, C., Vogel, A., Booth, I. and Martin, G.R. (1993) FGF-4 replaces the apical ectodermal ridge and directs outgrowth and patterning of the limb. *Cell*, **75**, 579–587.
77. Lussier, M., Canoun, C., Ma, C., Sank, A. and Shuler, C. (1993) Interdigital soft tissue separation induced by retinoic acid in mouse limbs cultured in vitro. *Int. J. Dev. Biol.*, **37**, 555–564.
78. Beverdam, A., Merlo, G.R., Paleari, L., Mantero, S., Genova, F., Barbieri, O., Janvier, P. and Levi, G. (2002) Jaw transformation with gain of symmetry after Dlx5/Dlx6 inactivation: mirror of the past? *Genesis*, **34**, 221–227.
79. Perera, M., Merlo, G.R., Verardo, S., Paleari, L., Corte, G. and Levi, G. (2004) Defective neuronogenesis in the absence of Dlx5. *Mol. Cell Neurosci.*, **25**, 153–161.
80. Simeone, A., Acampora, D., Pannese, M., D'Esposito, M., Stornaiuolo, A., Gulisano, M., Mallamaci, A., Kastury, K., Druck, T., Huebner, K. *et al.* (1994) Cloning and characterization of two members of the vertebrate Dlx gene family. *Proc. Natl Acad. Sci. USA*, **91**, 2250–2254.
81. Morsut, L., Yan, K.P., Enzo, E., Aragona, M., Soligo, S.M., Wendling, O., Mark, M., Khetchoumian, K., Bressan, G., Chambon, P. *et al.* (2010) Negative control of Smad activity by ectodermin/Tif1gamma patterns the mammalian embryo. *Development*, **137**, 2571–2578.
82. Zhadanov, A.B., Bertuzzi, S., Taira, M., Dawid, I.B. and Westphal, H. (1995) Expression pattern of the murine LIM class homeobox gene Lhx3 in subsets of neural and neuroendocrine tissues. *Dev. Dyn.*, **202**, 354–364.
83. Bendall, A.J. and Abate-Shen, C. (2000) Roles for Msx and Dlx homeoproteins in vertebrate development. *Gene*, **247**, 17–31.
84. Nellen, D., Burke, R., Struhl, G. and Basler, K. (1996) Direct and long-range action of a DPP morphogen gradient. *Cell*, **85**, 357–368.
85. Garaffo, G., Conte, D., Provero, P., Tomaiuolo, D., Luo, Z., Pinciroli, P., Peano, C., D'Atri, I., Gitton, Y., Etzion, T. *et al.* (2015) The Dlx5 and Foxg1 transcription factors, linked via miRNA-9 and -200, are required for the development of the olfactory and GnRH system. *Mol. Cell Neurosci.*, **68**, 103–119.